Ac susceptibility and ^{51}V NMR study of MnV_2O_4

2008 J. Phys.: Condens. Matter 20 135218

(http://iopscience.iop.org/0953-8984/20/13/135218)

J. Phys.: Condens. Matter **20** (2008) 135218 (6pp) doi:10.1088/0953-8984/20/13/135218

Ac susceptibility and ^{51}V NMR study of MnV_2O_4

S-H Baek[1,2], K-Y Choi[1], A P Reyes[1], P L Kuhns[1], N J Curro[2], V Ramanchandran[1], N S Dalal[1], H D Zhou[1] and C R Wiebe[1]

[1] National High Magnetic Field Laboratory, Tallahassee, FL 32310, USA
[2] Los Alamos National Laboratory, Los Alamos, NM 87545, USA

Received 4 January 2008, in final form 21 February 2008
Published 12 March 2008
Online at stacks.iop.org/JPhysCM/20/135218

Abstract

We report ^{51}V zero-field NMR of the manganese vanadate spinel compound, MnV_2O_4, together with both ac and dc magnetization measurements. The field and temperature dependences of ac susceptibilities show a re-entrant-spin-glass-like behavior below the ferrimagnetic (FEM) ordering temperature. The zero-field NMR spectrum consists of multiple lines ranging from 240 to 320 MHz. Its temperature and field dependences are discussed in terms of the persistence of a small fraction of the cubic phase within the FEM ordered ground state. Due to strong spin–orbit couplings the disordered phase induces an anomalous structural and electronic state in an external field. This suggests a close correlation between magnetism and structure.

(Some figures in this article are in colour only in the electronic version)

1. Introduction

For several decades, transition-metal spinel compounds of the AB_2X_4 type have been a subject of active research because of the intriguing nature of the underlying physics [1]. The many unusual phenomena found in the spinel compounds are due primarily to the corner-sharing tetrahedral network of the B cations, which resembles the geometrically frustrated pyrochlore lattice. The magnetic properties of spinels rely heavily on whether the B cations have orbital degrees of freedom, and whether the A cations are magnetic or non-magnetic.

Among the vast number of spinels, manganese vanadate MnV_2O_4 [2, 3] is one of the fascinating but more complex compounds because (i) the V^{3+} ion ($3d^2$, $S = 1$) possesses orbital degeneracy in its t_{2g} orbital, the orbital ordering being a common feature found in other insulating vanadates (A = Zn [4], Mg [5], Cd [6]), and (ii) both the A and B sites are magnetic as in manganese chromite, $MnCr_2O_4$ [7, 8].

One may expect that MnV_2O_4 shares common features with $MnCr_2O_4$ as well as with other vanadium spinels. Indeed, MnV_2O_4 undergoes long-range FEM ordering at 56 K and the spin configuration of the B sites changes from collinear to non-collinear triangular type at low temperature (T), as found in $MnCr_2O_4$ [8]. Like other vanadate spinels, MnV_2O_4 also undergoes two successive phase transitions—orbital order and magnetic long-range order. Interestingly, in the case of MnV_2O_4, the cubic-to-tetragonal structural transition related to the orbital order takes place at $T_S = 53$ K, just below the FEM transition temperature $T_C = 56$ K [3]. With magnetic field the structural phase transition temperature T_S shifts to higher temperature while accompanying a large change of lattice striction. This means that a field-induced switching of crystal structure takes place, indicating strong spin–orbital coupling. However, this issue has not yet been thoroughly addressed.

In this paper, we report the observation of the intriguing magnetic behavior in MnV_2O_4 through ac/dc magnetization and ^{51}V NMR measurements. The temperature and field dependence of the NMR spectrum shows that there exists an additional cubic phase on top of the long-range FEM order. The field-induced anomalies of the NMR spectrum suggest a change of local electronic and magnetic properties with external field, evidence that magnetism is linked to the structural phase transition.

2. Sample preparation and experimental details

A polycrystalline powder sample of MnV_2O_4 was prepared by a standard solid-state reaction. Stoichiometric mixtures of MnO and V_2O_3 were ground together and pressed into a pellet; the pellet was placed into an evacuated quartz tube ($\sim 10^{-5}$ Torr) and fired for 40 h at 950 °C. Samples were characterized by x-ray powder diffraction. Both dc and ac susceptibility measurements were performed as a function

of both field and temperature using a SQUID magnetometer (Quantum Design MPMS) over a range of 10^{-1}–10^{3} Hz with a driving field of 5 Oe. NMR experiments were carried out at zero external field using a coherent pulsed spectrometer capable of computer-controlled tuning of a probe which is calibrated over a wide frequency range. In preliminary measurements using an untuned NMR probe ($Q = 1$), we detected two groups of signals at near 280 and 560 MHz at 4.2 K. These were assigned to the NMR signals of V^{3+} and Mn^{2+} ions, respectively. A tuned circuit was employed subsequently to focus on the stronger signal of the V site. For detailed temperature dependent measurements the sample was cooled from room temperature to 4 K at two different rates: ~1 K min^{-1} for slow cooling (SC) and 60 K min^{-1} for rapid cooling (RC). NMR data were taken as the temperature was raised. The ^{51}V NMR spectra were obtained by integrating averaged spin echo signals as the frequency was swept through the resonance line. The spin echo is formed by the pulse sequence $\pi/2$–τ–$\pi/2$ with $\pi/2 \sim 2$ μs and $\tau \sim 20$ μs. We note that an optimal pulse does not vary appreciably over the whole frequency range. Thus, we fixed the pulse length to the value found at the center of the spectrum.

3. Results and discussion

3.1. Magnetic susceptibilities

Figure 1 shows the temperature dependence of the dc susceptibility under an applied field of 300 Oe together with the ac susceptibility at a frequency of 1 Hz. The field-cooled (FC) and zero-field-cooled (ZFC) curves display a pronounced bifurcation below the FEM ordering temperature of T_C. As T_C is approached from above, the FC curve increases steeply and then shows a dip around the structural phase transition temperature at T_S and finally increases monotonically. In contrast, the ZFC curve exhibits a maximum and then a monotonic decrease upon cooling from T_C. Our results are in a good agreement with [3]. Clearly, there is a remarkable difference between the ac and ZFC dc susceptibilities below T_C, suggesting the presence of re-entrant-spin-glass-(RSG-) like anomalies.

In figure 2 we present the temperature dependence of the ac susceptibilities, $\chi(H_a, T)$, for different static fields H_a applied parallel to the ac driving field. With decreasing temperature the real part of $\chi(H_a, T)$ exhibits a sharp peak around T_C and then a round maximum, and finally falls off upon further cooling. With increasing H_a, the latter maximum (designated by T_H) decreases in both amplitude and temperature. This so-called Hopkinson maximum arises from processes associated with the regular/technical contributions to the susceptibility (for example, domain wall motion and coherent rotation) [9]. The former sharp peak develops into two peaks (denoted by T_m and T_S, respectively) with increasing dc field. The peak T_m is suppressed in amplitude and shifts to higher temperature with an increase in the dc field. This is due to critical fluctuations accompanying a transition from a paramagnetic to an FEM state [10]. In contrast, the peak T_S decreases in amplitude without showing any shift in

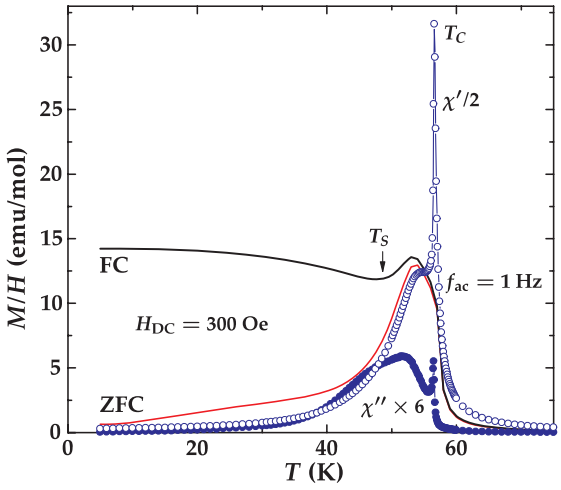

Figure 1. Temperature dependence of the ac (solid and empty circle symbols) and dc (solid lines) susceptibilities of MnV_2O_4. For clarity, the real and imaginary parts of the ac susceptibilities are rescaled by an arbitrary amount.

temperature. This might be associated with the structural phase transition [3]. The imaginary part of $\chi(H_a, T)$ shows a sharp peak around T_C, which exhibits a similar behavior as the peak T_S. In addition, there is the loss peak of $\chi''(H_a, T)$ at ~ 51 K, which is suppressed in both temperature and amplitude as H_a increases. This maximum and the absence of a clear cusp-like feature are incompatible with a canonical spin glass picture. Rather, the dominant contribution to the RSG-like anomalies is provided by the relaxation of the FEM domains, as we shall see later.

In the analysis of the susceptibility data we note that the peak T_m is governed by critical fluctuations, and may be expected to exhibit scaling behavior. The field and temperature dependences of the critical peak, $\chi_m = \chi(H_i, T_m)$, are related to the standard critical exponents [11–13] by

$$\chi(H_i, T_m) \propto H_i^{1/\delta - 1} \tag{1}$$

$$t_m \propto H_i^{(\gamma+\beta)^{-1}} \tag{2}$$

$$\chi(H_i, T_m) \propto t_m^{-\gamma}, \tag{3}$$

where H_i is the internal field given by $H_a = H_i - NM$, N is the demagnetizing factor and M is the magnetization. In our case, N is estimated by the slope of the low field shearing curves around T_C (not shown here). The parameter t_m is the reduced temperature defined as $t_m = (T_m - T_C)/T_C$. In figure 3 we provide a double-logarithmic plot of $\chi(H_i, T_m)$ versus H_i, t_m versus H_i and $\chi(H_i, T_m)$ versus t_m, respectively. We determine the temperature of $T_C = 56.58$ K from the zero-field data. The critical field amplitude $\chi(H_i, T_m)$ is directly obtained from figure 2(a). A close look at the data reveals a small curvature at low fields. This is typical for the system with exchange coupling strength disorder [10]. A least squares fit of the data between the restricted fields yields the exponent values of $\delta = 4.47 \pm 0.05$, $\gamma + \beta = 0.95 \pm 0.04$ and $\gamma = 0.59 \pm 0.03$. The δ and β values agree with the prediction of a 3D Heisenberg model; however, the γ value does not [12].

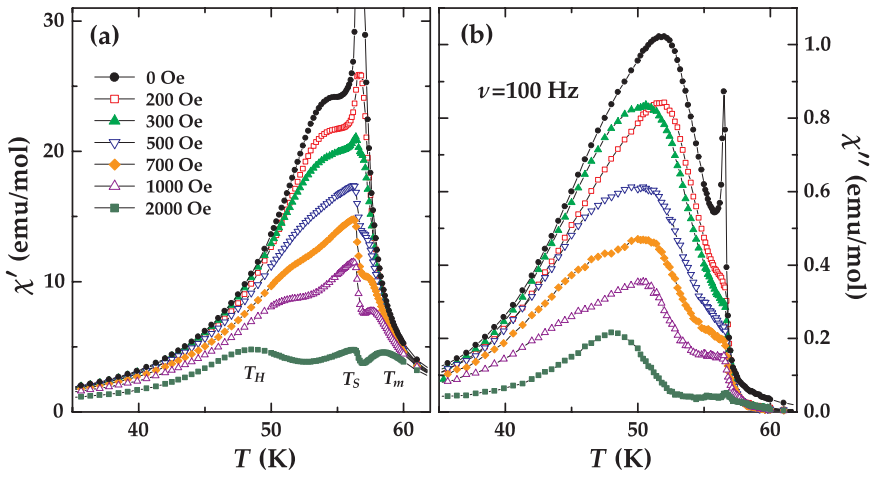

Figure 2. Field dependence of the real (a) and imaginary (b) parts of the ac susceptibility of MnV_2O_4 as a function of temperature. A field is driven at $H_{ac} = 5$ Oe and $\nu = 100$ Hz.

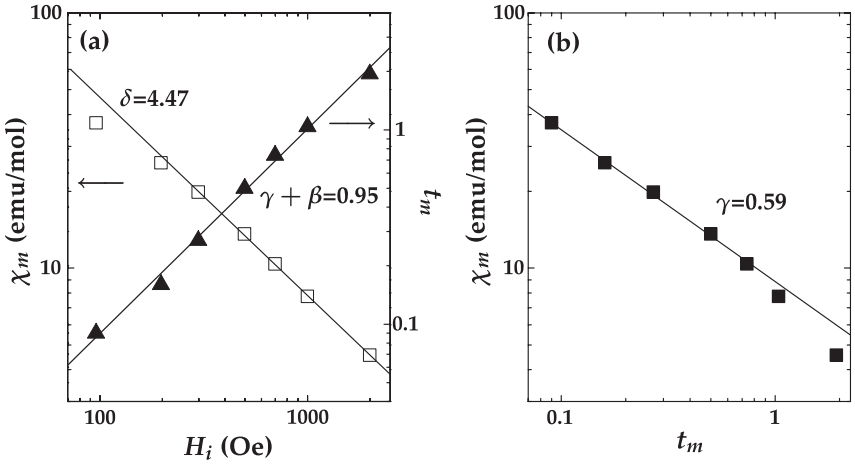

Figure 3. (a) The critical field amplitude versus the internal field (open square) is presented together with the reduced temperature versus the internal field (full triangle) on a double-logarithmic scale. (b) A double-logarithmic plot of the critical field temperature versus the reduced temperature. The solid and dotted lines are fits to equations (1)–(3).

Although we cannot exclude the uncertainties in evaluating exponents, it might be ascribed to a first-order-like transition due to strong spin–orbital coupling as well as to the persistence of a cubic phase below T_S (see below).

In figure 4 the temperature dependence of $\chi'(T)$ and $\chi''(T)$ is presented as a function of frequency in the range of 10^{-1}–10^3 Hz. Both $\chi'(T)$ and $\chi''(T)$ exhibit appreciable frequency dependence between 20 K and T_C. Overall, with increasing frequency both $\chi'(T)$ and $\chi''(T)$ shift to higher temperature. Below 20 K, no anomaly is detected in the ac susceptibility. This is due to the fact that the pinning barriers for the domains are too high for any significant contribution to the low field ac response.

Since there is no clear anomaly of $\chi'(T)$ at T_C and a broad maximum of $\chi''(T)$, we used the inflection point of $\chi'(T)$ to estimate the shift of the ac susceptibility as a function of the frequency (see the inset of figure 4(a)). From the maximal shift ΔT_i we obtain the value of $\varphi = \Delta T/T_i \Delta(\log\omega) \sim 0.007$. Although this value is rather close to that of a spin glass (of the order of 10^{-2}) [14], a fit to the Vogel–Fulcher law $\omega = \omega_0 \exp[-E_a/k_B(T_i - T_0)]$ yields the unrealistic values of $\omega_0 \approx 10^{33}$ Hz, $E_a \approx 287$ K, and $T_0 \approx 33.5$ K. This discrepancy suggests that the RSG-like anomalies are not related to a spin glass. Rather, recent x-ray diffraction [15] and neutron scattering results [16] uncovered the coexistence of a small fraction of the cubic phase in the tetragonal phase. In this light, the RSG-like anomalies can be attributed to (i) domain wall pinning effects due to the quenching of the disordered cubic phase, and (ii) the changes of the domain structure due to the temperature dependent fraction of the tetragonal phase. The former is correlated to the field dependent maximum at T_H while the latter to the field independent, giving rise to a sharp peak at T_S (see figure 2).

3.2. NMR measurements

Temperature dependent ^{51}V zero-field NMR spectra are shown in figure 5(a) for slow cooling, and in figure 5(b) for rapid cooling. The Boltzmann correction for the signal intensities has been made by multiplying each spectrum by T. The

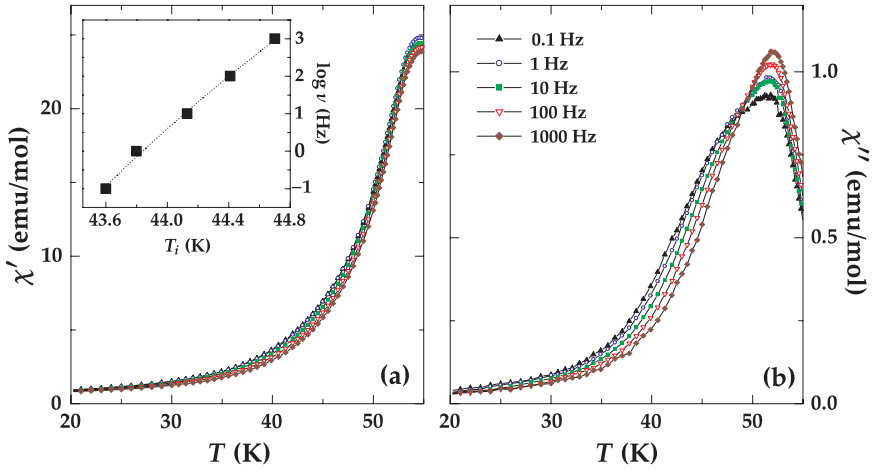

Figure 4. Frequency dependence of the real (a) and imaginary (b) parts of the ac susceptibility as a function of temperature. Inset: frequency shift of the inflection point of the real part of the susceptibility versus temperature.

spectrum has a complex structure and spans a wide range of frequencies from 240 to 320 MHz. The resonance frequency in zero external field is given as $\gamma_N H_{\rm hf}$ where γ_N (= 11.193 MHz T^{-1}) is the nuclear gyromagnetic ratio. The hyperfine field $H_{\rm hf}$ is dominated by the core polarization of the inner s electrons by the outer unpaired d electrons. For the V^{3+} ion ($3d^2$, $S = 1$), the estimated $H_{\rm hf}$ due to pure Fermi contact is about ∼25 T [17], which falls into ∼280 MHz range. The contributions from transferred, dipolar, or orbital hyperfine fields are negligible.

One can infer from figure 5 that the ^{51}V NMR line is composed of several overlapping structures, with peaks that are somewhat resolved. This structure is not surprising given the low crystal symmetry[3]. One possibility is that the quadrupole interactions split the ^{51}V ($I = 7/2$) degenerate levels, producing $2I = 7$ transitions. However, we discard this model since the quadrupole coupling required to represent the spectrum would be too large for the V nucleus. Hence, we attribute the structures to V sites belonging to different magnetic sites.

The temperature dependence of the integrated intensity multiplied by T of the spectrum is shown in figure 5(c) for both SC and RC. The signal for the RC case can be observed even above T_C, while the signal for SC becomes very weak near 40 K. Generally, the loss of NMR signal intensity near T_C is due to the critical spin fluctuations, which become much faster than the NMR timescale [18]. The different temperature dependence of the signal intensity of the same sample for different cooling rates is consistent with a quenching of a disordered state, in this case, the cubic FM phase being locked in below T_S [3].

By examining the evolution of the spectrum in figures 5(a) and (b), we note that the NMR peak near 270 MHz is quite distinguishable from the other lines, and survives after the disappearance of the other lines at high temperature. Single crystal data [19] indicate that most of the lines, including this 270 MHz line and the 305 MHz line, are unambiguously associated with the disordered states affected by the impurity cubic phase: the pure tetragonal phase gives rise to a narrow line near 280 MHz which is unresolved in this complex broad spectrum. The strong effect of the small mixed cubic phase on the NMR spectrum is not currently understood, but we conjecture that the cubic domain structure enhances the NMR signal more than the tetragonal domain does. Also we observe that the shift of the NMR line, if any, is very small up to temperatures near T_C. The NMR resonance frequency usually follows the bulk magnetization, which often shows gradual second order transition behavior. Therefore, the NMR data suggest that the magnetic transition at T_C must be of first order.

We turn next to the external field (H) dependence of the NMR spectrum, shown in figure 6. We observe that each identified line at zero field does not shift linearly with H. As the field increases, instead, the spectrum in the 250–290 MHz range is suppressed, while the spectrum in the 290–320 MHz range gains in intensity. Moreover, new NMR lines show up around 325 and 335 MHz above 3.5 T. It is not straightforward to extract useful information from such puzzling behavior. As a first approximation, we plot the first moment (M_1) or the center of gravity of the spectrum versus H in figure 6(c). The slope of M_1 versus H is initially 5.4 MHz T^{-1} but increases smoothly up to 3 T, being fixed to 7 MHz T^{-1}. The value is still smaller than the expected gyromagnetic ratio γ_N of V (11.193 MHz T^{-1}). The overall positive shift of the lines shows that the moment on the V sites is opposite to the net magnetization (since the hyperfine field is negative). We conjecture that this behavior may be possible only with assumption of discrete spin directions which are distributed spatially. The decrease of the slope below 3 T may be due to the change of the domain dynamics or the change of structure or electronic state in the external field.

We also observed that the total intensity of the spectrum increases with increasing H up to 4 T, above which it is saturated (see figure 6(b)). Typically, zero-field NMR signal decreases with increasing external field. This is due to the wipeout of the domain walls since the domain wall motion is the main contribution to NMR signal enhancement. Even in

[3] Fe^{57} NMR in Fe_3O_4 (magnetite) gave rise to 24 lines corresponding to the total number of Fe sites in the monoclinic unit cell at low temperature [22].

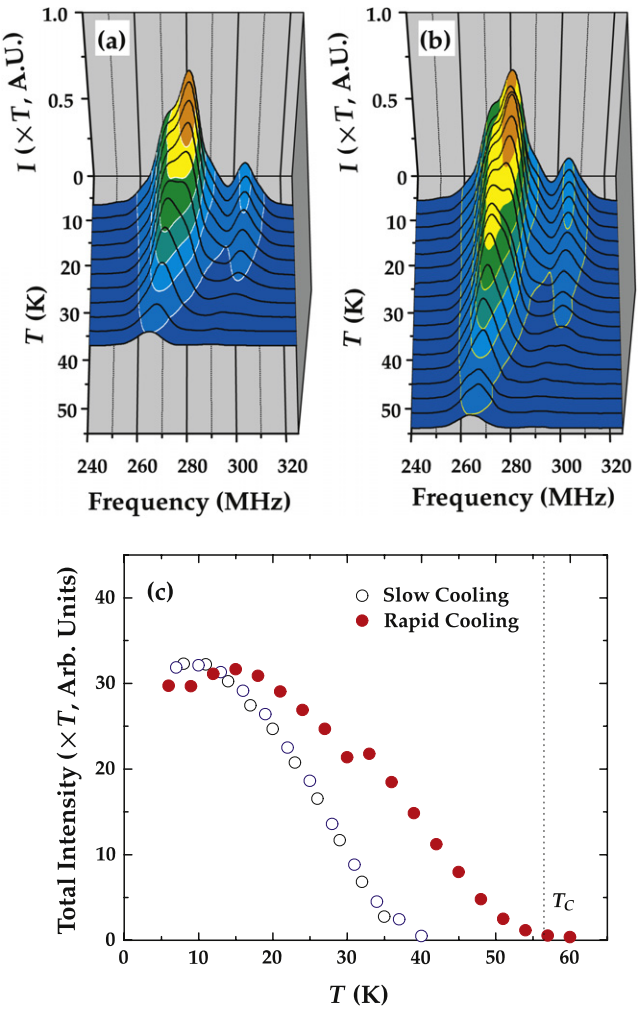

Figure 5. (a) Evolution of the NMR spectrum with increasing T in ZF for the slow cooling condition. The Boltzmann correction for intensity was taken into account by scaling each spectrum by T. (b) For rapid cooling, the evolution of the spectral shape is the same except the observation of the signal at much higher temperature. (c) Total integrated intensity of the NMR signal in zero field was plotted against temperature for slow and rapid cooling. Note that, for rapid cooling, the signal was detected even above T_C.

the case of coherent domain rotation, the enhancement should decrease because the external field adds to the anisotropy field to impede the ac electronic oscillation. This explains the regular decrease of the intensity observed at the low field. Thus, the unusual enhancement of the high-field signal suggests the development of a new local structure or electronic state with H, leading to a different spin susceptibility and enhancement factor.

Since the static magnetization curve shows no noticeable anomalies up to 6 T at 4.2 K, the character of the structural and electronic change of a ground state with H should be local rather than global. Accordingly, we rule out the transition between different long-ranged magnetic orders as a possible origin. We recall that the structural phase transition in MnV_2O_4 is a cooperative phenomenon governed by orbital degrees of freedom of the V site and that magnetic field induced switching of crystal structure appears [3]. We shall discuss the origin of the peculiar behavior of the field dependence of the NMR spectrum in terms of spin–orbital couplings.

Our compound has a spinel structure, which contain two different exchange coupling constants: J_{AB} and J_{BB} between the A and B and the B and B sites, respectively. For a cubic phase, a magnetic configuration relies on the parameter u defined as [20]

$$u = \frac{4J_{BB}S_B}{3J_{AB}S_A}, \tag{4}$$

where S_A and S_B are spin magnitudes at the respective A and B sites. The relative strength of two interactions determines a ground state. For example, the ground state of chromites $[Co,Mn]Cr_2O_4$ with $u = 1.5$–2.0 shows a coexistence of FEM long-range order and spiral short-range order that causes the RSG-like behavior [8]. The MnV_2O_4 system seems to lie in the same parameter range, as suggested by the fact that the RSG-like behavior starts to appear at T_C of the cubic phase (see figure 1).

In $[Co, Mn]Cr_2O_4$ the appearance of the short-range order is ascribed to the residual magnetic frustration in the B site, which is non-vanishing when J_{AB} is smaller than J_{BB}. In our case, however, this scenario is not relevant since the frustration could be relieved through the orbital ordering of the V^{3+} ions. In the cubic phase ($T > T_S$) the t_{2g} orbitals are degenerate and thus the orbital degrees of freedom are irrelevant. The V sublattice aligns ferromagnetically due to the antiferromagnetic couplings between V^{3+} and Mn^{2+} ions. In contrast, in the tetragonal phase ($T < T_S$), a structural phase transition takes place in which the orbital configuration is intimately coupled to a spin configuration via an orbital–spin coupling [3]. Recent x-ray diffraction [15] and neutron [16] measurements revealed the antiferro-orbital arrangement of the V^{3+} ions, where d_{xz} and d_{yz} orbitals are alternately occupied along the c axis. This is consistent with the model proposed by Tsunetsugu and Motome [21].

Previously, we mentioned that a small fraction of the cubic phase coexists with the main tetragonal phase below $T < T_S$. This is also supported by the cooling rate dependence of the NMR spectrum. In this situation, the local moment of the V ions will be distributed with the various angles as seen from the broad zero-field NMR spectrum. As a result, a small fraction of the cubic phase domain will be present in the tetragonal phase domains. Here we stress that the presence of a disordered cubic phase provides a good opportunity to address the field-induced aspect of a crystal structure. With applied magnetic field, the energy gain of the antiferro-orbital configuration becomes larger than the orbital-disordered one according to the Kugel–Khomskii theory. This leads to a switching of the cubic phase to the tetragonal one with increasing field H. The larger the magnetic field, the more the distorted crystal structure becomes stabilized. This will change the degree of the distribution of local fields and angles as a function of field. Finally, this leads to a change of the local spin susceptibility. Therefore, the field-induced anomalies of the NMR spectrum demonstrate the close correlation between the crystal structure and magnetism through spin–orbital couplings.

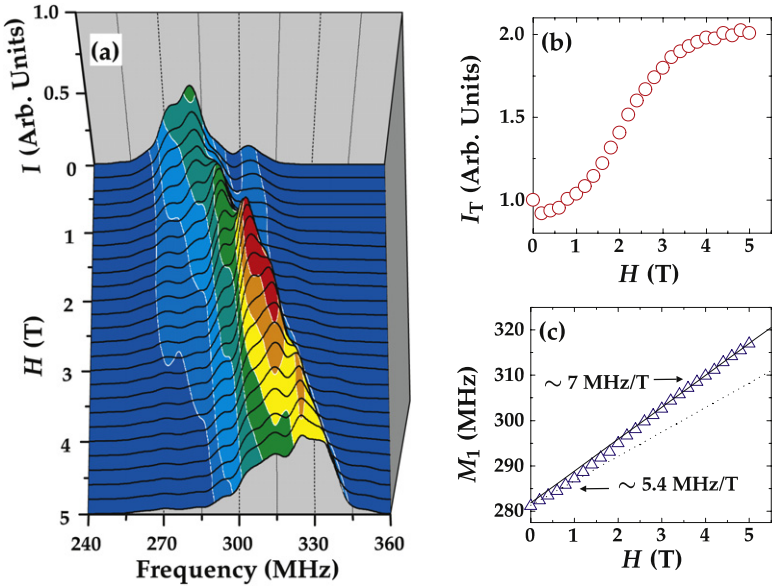

Figure 6. (a) External field dependence of spectrum up to 5 T. (b) Total integrated intensity increases with external field saturating at ∼4 T. (c) First moment versus external field. The initial slope of 5.4 MHz T^{-1} changes to 7 MHz T^{-1} at higher fields. The value must be compared to the expected value of 11.193 MHz T^{-1}.

4. Conclusion

In conclusion, we have investigated the magnetic properties of MnV_2O_4 through magnetization and NMR measurements. We have observed the re-entrant-spin-glass-like behavior as well as the appearance of the new NMR lines and the strong increase of the NMR intensity at high field. The field-induced anomalies are attributed to the intimate relation between magnetism and the orbital degrees of freedom and a small amount of a cubic phase in the tetragonal matrix.

Acknowledgments

This work was supported by NSF in-house research program State of Florida under cooperative agreement DMR-0084173. We appreciate a helpful discussion with M Hoch.

References

[1] Radaelli P G 2005 *New J. Phys.* **7** 53
[2] Plumier R and Sougi M 1989 *Physica* B **155** 315
[3] Adachi K, Suzuki T, Kato K, Osaka K, Takata M and Katsufuji T 2005 *Phys. Rev. Lett.* **95** 197202
[4] Lee S-H, Louca D, Ueda H, Park S, Sato T J, Isobe M, Ueda Y, Rosenkranz S, Zschack P, Iniguez J, Qiu Y and Osborn R 2004 *Phys. Rev. Lett.* **93** 156407
[5] Mamiya H, Onoda M, Frubayashi T, Tang J and Nakatani I 1997 *J. Appl. Phys.* **81** 5289
[6] Onoda M and Hasegawa J 2003 *J. Phys.: Condens. Matter* **15** L95
[7] Hastings J M and Corliss L M 1962 *Phys. Rev.* **126** 556
[8] Tomiyasu K, Fukunaga J and Suzuki H 2004 *Phys. Rev.* B **70** 214434
[9] Chikazumi S 1997 *Physics of Ferromagnetism* (Oxford: Clarendon)
[10] Williams G 1991 *Magnetic Susceptibility of Superconductors and Other Spin Systems* ed R A Hein (New York: Plenum)
[11] Stanley H E 1971 *Introduction to Phase Transitions and Critical Phenomena* (Oxford: Clarendon)
[12] Campostrini M, Hasenbusch M, Pelissetto A, Rossi P and Vicari E 2002 *Phys. Rev.* B **65** 144520
[13] Zhao H H, Kunkel H P, Zhou X Z, Williams G and Subramaniam M A 1999 *Phys. Rev. Lett.* **83** 219
[14] Mydosh J A 1993 *Spin Glasses: An Experimental Introduction* (London: Taylor and Francis)
[15] Suzuki T, Katsumura M, Taniguchi K, Arima T and Katsufuji T 2007 *Phys. Rev. Lett.* **98** 127203
[16] Garlea V O, Jin R, Mandrus D, Roessli B, Huang Q, Miller M, Schultz A J and Nagler S E 2007 *Preprint* cond-mat/0711.1844
[17] Freeman A J and Watson R E 1965 *Magnetism IIA* ed G T Rado and H Suhl (New York: Academic)
[18] Curro N J, Hammel P C, Suh B J, Hücker M, Büchner B, Ammerahl U and Revcolevschi A 2000 *Phys. Rev. Lett.* **85** 642
[19] Baek S-H, Choi K-Y, Reyes A P, Curro N J, Dalal N S, Zhou H D and Wiebe C R 2008 at press
[20] Menyuk N, Dwight K, Lyons D and Kaplan T A 1962 *Phys. Rev.* **127** 1983
[21] Tsunetsugu H and Motome Y 2003 *Phys. Rev.* B **68** 060405(R)
[22] Novák P, Štěpánková H, Englich J, Kohout J and Brabers V A M 2000 *Phys. Rev.* B **61** 1256